Published in final edited form as:
Neurosurgery. 2009 April ; 64(4): 622–631. doi:10.1227/01.NEU.0000341529.11231.69.

Influence of Intracranial Aneurysm-to-Parent Vessel Size Ratio on Hemodynamics and Implication for Rupture: Results from a Virtual Experimental Study

Markus Tremmel, Ph.D.,
Department of Neurosurgery, University at Buffalo, State University of New York, and Millard Fillmore Gates Hospital, Kaleida Health, Buffalo, New York

Toshiba Stroke Research Center, School of Medicine and Biomedical Sciences, University at Buffalo, State University of New York

Sujan Dhar, M.S.,
Department of Mechanical and Aerospace Engineering, University at Buffalo, State University of New York, Buffalo, New York

Toshiba Stroke Research Center, School of Medicine and Biomedical Sciences, University at Buffalo, State University of New York

Elad I. Levy, M.D.,
Departments of Neurosurgery, and Radiology, University at Buffalo, State University of New York, and Millard Fillmore Gates Hospital, Kaleida Health, Buffalo, New York

Toshiba Stroke Research Center, School of Medicine and Biomedical Sciences, University at Buffalo, State University of New York

J Mocco, M.D., M.S., and
Department of Neurosurgery, University at Buffalo, State University of New York, and Millard Fillmore Gates Hospital, Kaleida Health, Buffalo, New York

Toshiba Stroke Research Center, School of Medicine and Biomedical Sciences, University at Buffalo, State University of New York

Hui Meng, Ph.D.
Departments of Neurosurgery and Mechanical and Aerospace Engineering, University at Buffalo, State University of New York, and Millard Fillmore Gates Hospital, Kaleida Health, Buffalo, New York

Toshiba Stroke Research Center, School of Medicine and Biomedical Sciences, University at Buffalo, State University of New York

Abstract

OBJECTIVE—The effectiveness of intracranial aneurysm (IA) size as a predictor for rupture has been debated. We recently performed a retrospective analysis of IA morphology and found that a new index, namely, aneurysm-to-parent vessel size ratio (SR), was strongly correlated with IA

Reprint requests: Hui Meng, Ph.D., Toshiba Stroke Research Center, University at Buffalo, State University of New York, 447 Biomedical Research Building, Buffalo, NY 14214. huimeng@buffalo.edu.
Markus Tremmel, Ph.D., and Sujan Dhar, M.S., contributed equally to this work.

Supplemental digital content is available for this article. Direct URL citations appear in the printed text and are provided in the HTML and PDF versions of this article on the journal's Web site (www.neurosurgery-online.com).

rupture, with 77% of ruptured IAs showing an SR of more than 2, and 83% of unruptured IAs showing an SR of 2 or less. As hemodynamics have been implicated in both IA development and rupture, we examine how varying SR influences intra-aneurysmal hemodynamics.

METHODS—One sidewall and 1 terminal IA were virtually reconstructed from patient 3-dimensional angiographic images. In 2 independent in silico experiments, the SR was varied from 1.0 to 3.5 by virtually changing either aneurysm size or vessel diameter while keeping the other parameter constant. Pulsatile computational fluid dynamics simulations were performed on each model for hemodynamics analysis.

RESULTS—Low SR (≤2) aneurysm morphology consistently demonstrated simple flow patterns with a single intra-aneurysmal vortex, whereas higher SR (>2) aneurysm morphology presented multiple vortices and complex flow patterns. The aneurysm luminal area that was exposed to low wall shear stress increased with increasing SR. Complex flow, multiple vortices, and low aneurysmal wall shear stress have been associated with ruptured IAs in previous studies.

CONCLUSION—Higher SR, irrespective of aneurysm type and absolute aneurysm or vessel size, gives rise to flow patterns typically observed in ruptured IAs. These results provide hemodynamic support for the existing correlation of SR with rupture risk.

Keywords

Intracranial aneurysm; Morphology; Parent vessel diameter; Rupture risk; Size ratio

---

Most clinical studies attempting to stratify the rupture risk of an intracranial aneurysm (IA) have relied on absolute aneurysm size as the primary metric for IA morphology (18,20,31, 41). Recent large- scale studies, such as the International Study of Unruptured Intracranial Aneurysms (18,41), have generated considerable controversy (2,9,10,12,21,26) as a result of predicting extremely low rupture rates on the basis of IA size. Numerous studies have disputed the application of size as a predictor of IA rupture risk, pointing out the frequency of subarachnoid hemorrhage from small aneurysms (3,6,13,28).

Location-based studies have consistently shown that certain parts of the cerebral vasculature, such as the posterior communicating artery and the anterior communicating artery (AComA), have a higher incidence of ruptured aneurysms when compared with other locations, such as the cavernous segment of the internal carotid artery (ICA) (3,6,13,28,35,39,40). It has also been noted that specific locations on the cerebral vasculature (e.g., AComA) harbor a high percentage of all small ruptured IAs; whereas at other locations (such as the ICA), small, ruptured IAs are substantially less frequent (3,6,13,28). These observations suggest that IA size loses relevance to rupture risk if location is not accounted for. Furthermore, it is likely that the variability of the rupture risk of different locations may be related to the caliber of the originating, or parent, vessel, resulting in higher risks for small- diameter vessels (e.g., AComA or posterior communicating artery) and lower risks for larger- diameter vessels (e.g., ICA) (3,6,13,28,35,39,40). Evaluation of the contribution of parent vessel geometry to aneurysm rupture risk may help resolve the above-noted conflicts regarding the use of IA size alone as a predictor of rupture risk.

In a recent study, we proposed a new parameter, size ratio (SR), defined as maximum aneurysm height/average parent vessel diameter, that incorporates the IA parent vessel geometry into a morphological index (11). That study compared SR with previously identified parameters, such as aneurysm size, aspect ratio, undulation index, ellipticity index, and non-sphericity index, and found SR to have the strongest correlation with IA rupture.

It has been hypothesized that the mechanism by which IA morphology relates to IA rupture is via the intra- aneurysmal hemodynamic environment created by a particular geometry (36).

Several studies have evaluated the relationship between intra- aneurysmal hemodynamics and IA growth rate and rupture risk (8,15–17,19,23–25,32,33,36). Computational fluid dynamics (CFD) studies of intra- aneurysmal hemodynamics have identified certain flow characteristics to be specific to ruptured aneurysms and, therefore, classified as potentially "dangerous" (8, 32,36). Regions of markedly low (<0.5 Pa) wall shear stress (WSS) on the IA inner wall, focused flow impingement zones, and complex flow patterns with features such as multiple vortices and creation and destruction of vortices during the cardiac cycle have all been identified as being more prevalent in ruptured IAs (8,32,36).

Because SR has been shown to correlate with IA rupture (11), we now investigate the effect of SR on intra-aneurysmal hemodynamics to elucidate the specific flow patterns that are prevalent in rupture- prone IAs. We performed pulsatile CFD simulations on 2 types of saccular IAs (sidewall and terminal) while virtually modifying the relationship between the IA and parent vessel, thereby allowing computational simulation of IA hemodynamics on preexisting aneurysms with constant morphology—except for a varying SR. Each original IA model was morphed to change only SR while keeping all other shape metrics constant. For the original IA models, we used anatomically accurate geometries reconstructed from patient 3-dimensional angiography rather than idealized models. Both original IAs were unruptured. The intent of this virtual analysis was to gain insight concerning the relationship between SR and hemodynamic environments associated with elevated IA rupture risk, thereby highlighting the importance of considering both aneurysm and parent vessel anatomy when assessing IA rupture risk.

MATERIALS AND METHODS

Selection of Aneurysm Geometries

From a cohort of 85 patients who underwent diagnostic 3-dimensional rotational angiography, 45 intracranial aneurysm images were reviewed that were of sufficient quality for accurate 3-dimensional reconstruction using in- house software based on open- source Visualization Toolkit libraries (http://www.vtk.org/). These 45 IAs, which included both ruptured and unruptured IAs, formed the basis for our previous morphology- rupture risk analysis (11), and they provided the model selection parameters for the current study as well. Morphological metrics were calculated for these 45 IAs, including aneurysm size (maximum perpendicular distance of the dome from the neck plane [30]), aspect ratio (ratio of the maximum perpendicular height to the average neck diameter [36,39]), undulation index (30), ellipticity index (30), nonsphericity index (30), and SR (maximum aneurysm height/average parent vessel diameter [11]). In cases of a terminal aneurysm, the parent vessel diameter in the calculation of SR was taken as the average of all 3 bifurcation branches (11). Averages of the above metrics were obtained, and 2 representative IAs (1 saccular sidewall and 1 saccular terminal) with morphologies that most closely approximated the averages were then chosen from the patient group. The 2 selected IAs were chosen a priori, and the proceeding virtual analysis was performed on these 2 aneurysms alone (i.e., these data do not reflect post-analysis selection bias). Coincidentally, both aneurysms were originally in the posterior circulation. The chosen sidewall IA was located on the posteroinferior cerebellar artery, and the chosen terminal IA was located on the basilar tip. Approval for the collection and review of the angiogram data was obtained from the Institutional Review Board at the University at Buffalo.

Original Geometries

The chosen original sidewall IA had a maximum height of 5.12 mm and an average parent vessel diameter of 2.5 mm, thereby giving an SR of 2.0. The original terminal IA had a maximum height of 3.6 mm with an average parent vessel diameter of 2.4, thereby giving an SR of 1.5. Additionally, both cases had an aspect ratio of 1.4. Both aneurysms were unruptured.

Parametric Modeling for Varying SR

To elucidate the relative importance of the parameter SR to the development of previously defined "dangerous" intra-aneurysmal hemodynamics (8,32,36), we performed pulsatile CFD analysis (detailed below) on the original 2 chosen representative IA cases and on a series of additional models that were created from the 2 original cases and in which we virtually manipulated the SR while keeping other morphological metrics (aspect ratio, undulation index, nonsphericity index, and ellipticity index) constant. In this way, confounding influences from other parameters were eliminated, and the influence of SR alone on hemodynamics could be assessed. It is important to note that the virtual manipulation aims to create a series of preexisting IAs of different size ratios. It does not aim to simulate a change in vessel size or aneurysm size over time in a particular patient. Virtual manipulation was performed by separating the IA sac and parent vessel using cutting tools on Ansys ICEM CFD software (Ansys, Inc., Canonsburg, PA) and then scaling the IA and parent vessel sizes up or down while holding their shapes constant. Once the newly scaled geometries were created, the models of the IA and vessel were merged again using Pro/Engineer (PTC, Needham, MA) to generate models of varying SRs for each patient case. Each IA model (terminal and sidewall) underwent 2 independent in silico experimental analyses. In experiment 1, the aneurysm size was kept the same as the original IA. The vessel diameter was scaled up or down to generate a range of different SRs. In experiment 2, the vessel diameter was kept the same as in the patient geometry. The aneurysm size was scaled up or down to generate a range of different SRs.

Cases with SRs of 1, 1.5, 2, 2.8, and 3.5 were thus created (Figs. 1 and 2). These SRs were chosen to span the range of 1 to 3.5 that we observed in our source population of 45 IAs, as well as to include the original 2 geometries from the representative patient sidewall (SR = 2.0) and terminal (SR = 1.5) IAs.

Numerical Simulation

Finite volume tetrahedral meshes consisting of approximately 200 000 to 1 million tetrahedral and wall prism elements (for accurate boundary layer resolution) were created for each model using Ansys ICEM CFD software. Numerical solution of the incompressible transient Navier-Stokes equations was obtained using the solver Star-CD (CD Adapco, Melville, NY). Inlet flow Reynolds numbers ($Re = \rho Ud/\mu$, where Re is the Reynolds number, ρ is the density, U is the average inlet velocity, d is the vessel diameter, and μ is the viscosity) were calculated from typical values of velocities and vessel diameters (1,6,38) at the locations of the 2 original IAs. The resulting Reynolds number was 380 for the sidewall IA and 272 for the terminal IA. At the model inlets for each patient case, pulsatile boundary conditions using this mean Reynolds number were implemented as SR was varied. The shape of the pulsatile waveform was obtained from transcranial Doppler ultrasound measurements on a normal subject. Although the shape of the waveform was held constant for each of the simulations, its velocity magnitude was scaled to the desired mean Reynolds number. It should be noted that the hemodynamic comparisons that follow will focus on qualitative flow changes with varying SR. Exact flow velocity values (and shape of the waveform) may vary based upon the assumptions of the model; however, the observed trends are expected to be maintained across model assumptions.

Blood was modeled as a Newtonian fluid (4,7) with a density of 1056 kg/m^3 and a viscosity of 0.0035 kg/ms. To ensure that numerical stability had been reached, 3 pulsatile cycles were simulated, with only the last cycle being used for output of results and post-processing. The CFD solution was output at 46 equally spaced time points through the third cycle. Owing to the lack of information on vessel properties such as elasticity and composition, the wall distensibility was neglected, and rigid wall boundaries with no-slip conditions were implemented at the vessel walls (7). This rigid wall assumption is acceptable for our analysis because the influence of wall compliance on the aneurysmal flow pattern is insignificant

compared with that of overall morphology (7). To provide a clear picture of the flow, all data are presented as the time-average of the solution over the third pulsatile cycle. For additional visualization, animations of the pulsatile flow field were also generated. Traction-free boundary conditions were implemented at the outlet (7,33), and in the terminal IA case, the flow was assumed to split according to the left and right posterior cerebral artery outlet areas, respectively.

Wall Shear Stress Comparison

In experiment 1, vessel size was scaled up or down to generate the desired SR, and a constant Reynolds number inlet boundary condition was imposed, which ensured similar flow patterns in all parent vessels. Consequently, flow velocity in each vessel must vary, causing larger vessel sizes to have lower velocities (and lower WSS) and vice versa for smaller vessels. To make WSS comparable in experiment 1, we normalized the WSS in each simulation and then rescaled it to the WSS level of the original patient IA case by defining

$$\mathrm{WSS}_{\mathrm{scaled}}=\mathrm{WSS}_{\mathrm{normalized}}\times(\rho U_{\mathrm{p}}{}^{2})=[\mathrm{WSS}/(\rho U^{2})]\times(\rho U_{\mathrm{p}}{}^{2}) \quad \text{(Eq 1)}$$

where ρ is the density, U is the average vessel velocity at the inlet (based on the mean Reynolds number), and the subscript "p" denotes the original patient (baseline) case. Plotting the scaled WSS, the parent vessels in all models assume the same value as in the original IA case, which allows easy comparison of WSS between the models.

In experiment 2, the above Reynolds number scaling procedure was not necessary because the vessel size was kept constant. Thus, all vessels had the same Reynolds number and the same flow velocity, and we have WSS = $\mathrm{WSS}_{\mathrm{scaled}}$.

To quantify "low" WSS regions in different cases, we compared the areas of the IA wall that had a $\mathrm{WSS}_{\mathrm{scaled}}$ (experiment 1) or WSS (experiment 2) lower than 0.5 Pa, which has been reported as a WSS value below which atherosclerotic degeneration, macrophage infiltration, and wall tissue inflammation are likely to occur (22,32). It has been noted that a WSS of 2 N/m^2 is suitable to maintain the structure of arterial vessels (22). An excessively low WSS (<0.5 Pa) has also been previously identified as a possible reason for degeneration and structural fragility of the aneurysm wall (32). All areas are reported in terms of percentage of the total IA area, which allows for easy comparison between experiment 1 and experiment 2 (where aneurysm sizes vary).

RESULTS

Experiment 1

For the models in experiment 1 (constant IA size), velocity vectors of the average flow were plotted on representative planes cut through the aneurysm volume (sidewall IA [Fig. 3A] and terminal IA [Fig. 3B]). The location of each cut plane was not constant but was chosen to best illustrate the intra-aneurysmal flow patterns. For both aneurysm types, vortex structures in the models with SRs of 1, 1.5, and 2 remained relatively simple, with a single prominent vortex inside the aneurysm volume. However, for models with SRs of 2.8 and 3.5, the flow pattern changed considerably, presenting more complex flow structures with multiple associated vortices. Animations of the flow vectors over the pulsatile cardiac cycle (see Videos, Supplementary Digital Content 1, http://links.lww.com/A779, and Supplementary Digital Content 2, http://links.lww.com/A780) further illustrate the complexity of the transient flow patterns. In a majority of the high SR cases, dynamically changing vortex patterns are observed

over the cardiac cycle. The low SR cases, on the other hand, present a stable, single vortex. This was consistent in both the sidewall and terminal IA cases.

Figure 4 shows the regions of low WSS_{scaled} on the aneurysmal surface for sidewall IA (Fig. 4A) and terminal IA (Fig. 4B). As SR increased, so did the IA inner-wall area that experienced low WSS_{scaled}, regardless of aneurysm type. The area of WSS_{scaled} of less than 0.5 Pa, given as the percentage of total IA area, is shown in a bar plot for each aneurysm type as a function of SR. This area increases sharply as SR increases beyond a value of 2, and it is interesting to note that the plots for both sidewall and terminal IAs show a very similar qualitative trend despite the vastly different aneurysm geometries.

Experiment 2

For the models in experiment 2 (constant vessel caliber), velocity vectors of the average flow were again plotted on representative cut planes that best illustrated the intra-aneurysmal flow structures (sidewall IA [Fig. 5A] and terminal IA [Fig. 5B]). Regardless of aneurysm type, flow patterns changed with increasing SR from a simple, single vortex to multiple vortices with an apparent threshold at an SR of 2, similar to the results observed in experiment 1. Online animations show the flow vectors over 1 pulsatile cardiac cycle for the sidewall IA (see Video, Supplementary Digital Content 3, http://links.lww.com/A781) and terminal IA (see Video, Supplementary Digital Content 4, http://links.lww.com/A782). As in experiment 1, complex and dynamic vortices are observed in the high SR cases, whereas the low SR cases present a simpler flow with a single, stable vortex.

Figure 6 shows the regions of low WSS on the aneurysmal surface for sidewall IA (Fig. 6A) and terminal IA (Fig. 6B). As the SR increases, we observe larger regions of low WSS, consistent with the results of experiment 1. The percentage area of WSS of less than 0.5 Pa is again shown in a bar plot, and as in experiment 1, the area increases sharply for both aneurysm types as SR increases beyond a value of 2.

DISCUSSION

We demonstrate that, while holding all other morphological parameters constant (including IA size, aspect ratio, and undulation index), modifying the SR alone is sufficient to create an intra-aneurysmal hemodynamic environment associated with ruptured IAs. This strongly suggests that the absolute size of an IA is less relevant to the development of dangerous intra- aneurysmal hemodynamics than is the relationship between IA size and parent vessel caliber (quantified by SR). The most widely studied morphological parameters, IA size and aspect ratio, account for the aneurysm, but not for parent vessel anatomy (3,6,28,30,37,39). Our results indicate that the relationship between IA size and parent vessel caliber is critical to the type of intra-aneurysmal hemodynamics generated, even when absolute IA size and other IA- specific morphological parameters are held constant.

In a study previously performed by our group on the same 45 patient IA geometries, the statistical correlation of various morphology parameters with IA rupture was investigated retrospectively (11). Those parameters included absolute IA size, aspect ratio, undulation index, ellipticity index, nonsphericity index, SR, and aneurysm/vessel angle. Among these, SR was found to have the most significant correlation with IA rupture ($P < 0.00026$; odds ratio, 1.14; 95% confidence interval, 1.03–1.92). The optimal threshold of SR was found to be 2.05, with 77.27% of all ruptured IAs having an SR of more than 2.05 and 83.21% of all unruptured IAs having an SR of 2.05 or less. The current flow dynamics study does not attempt to statistically correlate SR with rupture. However, we do note that the CFD results observed are consistent with the findings of the previous statistical study and lend credence to the value of SR as a morphological parameter. When SR exceeds 2, the simple, stable vortex patterns turn

into complex patterns with multiple vortices that change dynamically during the course of a cardiac cycle. Such complex flow patterns and dynamic creation and destruction of vortices have previously been associated with ruptured IAs (8,36). In the current study, we also observed a noticeable increase in the percentage of IA area exposed to low WSS or WSS_{scaled} once SR becomes greater than 2. This is consistent with studies that found large areas of low WSS to correlate with IA growth (19) and rupture (32,36). The trends observed in our experiments are similar for the sidewall and terminal models, indicating that SR remains relevant through large variations in IA and environment morphologies.

Various studies have reported a rupture relationship with IA location (3,6,13,28,35,39,40), fueling the arguments of those criticizing large clinical trials that stratified IAs at different locations according to size alone. In particular, the AComA, which is a small- caliber vessel, has been identified as a location portending high rupture risk, even for small aneurysms (3,6, 13,28). In fact, 94.4% of all AComA aneurysms have been found to be less than 10 mm in size (13,40) but nevertheless comprise 30% to 32% (28,35) of all ruptured IAs. On the other hand, it has been observed that the ICA, a large- caliber vessel, accounts for a large percentage of all unruptured IAs (13,35,39,40). The high incidence of small ruptured IAs at the AComA is consistent with the observation by Carter et al. (6) that the average size of ruptured IAs is smaller on vessels of smaller sizes, because location is closely related to vessel diameter, ranging from 1.25 mm at the AComA to 4 mm at the ICA on average (38). From these findings, it is evident that size alone is insufficient to accurately predict IA rupture risk. To improve the prediction of rupture risk, the IA location with its specific parent vessel diameter must also be accounted for. A parameter like SR can potentially achieve this, because a high- risk IA of a given SR will have a smaller absolute size on the AComA than on the ICA (i.e., an SR of 3 would typically correspond to an aneurysm size of approximately 3.75 mm on the AComA versus approximately 12 mm on the ICA). In the current CFD study, an increased SR created flow patterns previously associated with rupture, which supports SR as a promising parameter. Additionally, we anticipate the applicability of SR to clinical practice to be aided by the relative ease by which it is calculated. With only standard tools and simple arithmetic, the SR of an IA can be generated in the space of a few seconds. This added benefit may encourage the use of SR by a wide sampling of clinicians, in contrast to other more complex IA parameter assessments.

It must be pointed out, however, that we only focused on the 2 main IA types (sidewall and terminal) in the current study, while keeping location and all shape-related factors (aspect ratio, undulation index, and so forth) constant. This procedure allows isolating the specific influence of SR on hemodynamics. However, it limits the generalization of the results. AComA aneurysms, in particular, have complicated inflow conditions, and the CFD results for terminal IAs presented here may not fully reflect the complex flow in all AComA IAs. One sidewall and 1 terminal case—i.e., the most common forms of IA—were chosen for a “first look” at how SR can affect intra- aneurysmal flow. A more comprehensive parametric study could be performed in the future by choosing a larger set of IAs from various locations and with varying shapes and running CFD for a series of virtual SR variations for each IA. However, because of the multitude of possible variations, this would be a large undertaking and exceeds the scope of the present article.

Although we demonstrated the significance of SR on intra- aneurysmal hemodynamics in the current study, this is not to suggest that absolute IA size is irrelevant. In fact, numerous studies have observed a connection between absolute IA size and rupture risk (18,20,31,41). However, as experiment 2 confirms, absolute IA size likely acts as a surrogate marker for SR in vessels of similar size and therefore would just as similarly predict intra-aneurysmal hemodynamics. It is therefore probable that studies primarily utilizing absolute IA size to assess rupture risk are using a nonideal categorization schedule should they stratify, for example, large-parent-

vessel 6-mm IAs with small-parent-vessel 6-mm IAs. In such cases, the first IA (low SR) would be grouped with the second IA (large SR), thereby overestimating the rupture risk of the former and underestimating the rupture risk of the latter.

CFD studies of parametric variation of IA morphology and its effect on intra-aneurysmal hemodynamics have been previously conducted (5,14,16,17,29). However, most of those studies used idealized aneurysm models (whether virtual, mechanical, or surgically created in animals), and the relevance of hemodynamics observed in idealized geometries to patient-specific aneurysm cases is questionable. To avoid this potential confounder, we used aneurysm models generated from actual human IAs, which provides an additional degree of confidence in the relevance of the hemodynamic features observed. Additionally, our investigation is the first, to our knowledge, to specifically evaluate the relationship of parent vessel size to aneu rysm size through our virtual manipulation of the SR. Previous assessments of parent vessel contribution to IA hemodynamics have focused on aneurysm orientation (i.e., sidewall, sidewall with branching vessel, and terminal) (16,17), rather than the relationship between parent vessel and aneurysm size.

Study Limitations

A significant limitation of this investigation is the small sample size. However, it is our intent to provide an illustrative investigation into the effect of a novel IA morphological parameter, SR, on hemodynamics—while holding other parameters constant. As a comprehensive assessment of the myriad of anatomic variants would be prohibitive, we believe that such a limited “first look” is an appropriate starting point. Additionally, we hope that these findings encourage future investigation into the more expansive aspects of elucidating the relationship between SR and IA rupture.

The original 2 aneurysm models (sidewall and terminal) were reconstructed from actual patient IA geometries. Although this is preferable to using idealized IA shapes, we acknowledge that our subsequent virtual manipulation (scaling of vessel caliber or aneurysm size) to create models of varying SRs is a simplified approach and should only be considered as a first step. In the future, the results from the present study need to be corroborated by analyzing a considerable quantity of real patient geometries that naturally have different SRs and performing CFD simulations on these subjects. This would be a huge undertaking, as other morphology parameters (including aspect ratio, undulation index, and vessel and aneurysm angles) would change along with SR in these geometries, and the influence of SR alone would be hard to isolate. Thus, many more patient cases would be required, and statistical tools would be needed to differentiate the influence of all parameters. We hope that the present findings will provide the impetus to allow such further investigations.

An additional limitation of the present study is the use of a representative normal subject waveform for our simulations. This was done because of the difficulty in obtaining waveforms for vessel locations deep in the brain and because these waveforms will vary not only from individual to individual but also owing to the physical, as well as the mental, activity of the subject (27,34). However, it has been demonstrated that the CFD solution is less sensitive to changes in the waveform than to changes in the overall aneurysm plus vessel geometry. Therefore, the error involved in using a representative waveform in the current study is expected to be small. Further simplifying model assumptions like Newtonian flow and the choice of “typical” flow Reynolds numbers from the literature will also undoubtedly influence quantitative CFD results. However, the current study investigates qualitative changes such as flow patterns, vortex dynamics, and wall exposure to low WSS with varying SR. Such changes are expected to follow the same trends, even if somewhat different flow parameters are chosen. Because actual patient velocity measurements were not available to calculate Reynolds

numbers in the present study, we believe that choosing values available in the literature was the best alternative.

We acknowledge that in our assessment of the WSS results, the value of 0.5 Pa chosen as a threshold for “low” WSS is somewhat arbitrary (although supported in the literature) (22,32) and should only be viewed as a tool for comparing the various models. If a different value (e.g. 1.0 Pa) had been chosen, the bar plots in Figures 4 and 6 would have different absolute values, but the qualitative trend (greater area of low WSS with increasing SR) would be the same.

It should also be noted that, although this study was prospective and experimental in nature, much of the supportive literature regarding the relationship of IA morphology and IA hemodynamics with IA aneurysm rupture is retrospective and, as a result, is dependent on critical assumptions. These include the assumption that postrupture aneurysm morphology is the same, or comparable, to prerupture morphology, as well as the assumption that an unruptured aneurysm is not in a state of imminent rupture. Although these assumptions do not directly confound our experimental investigation, they are fundamental to the referenced literature as well as to the suggested implications of our findings.

Finally, it must be pointed out that biological and environmental factors (such as smoking, hypertension, sex, and age) play an important role in the pathological history of aneurysms. The goal of the current study was to examine variation in hemodynamics when a specific morphological metric, SR, was varied. Studies of the effects of the above- listed additional factors on IA rupture can provide valuable insight into IA behavior; however, they are beyond the scope of this study.

CONCLUSION

Previous large clinical investigations have focused on IA size as being critical to rupture risk. The interpretation of the results of these studies may be confounded owing to the grouping of small aneurysms on large vessels with those of small aneurysms on small vessels. In this study, we demonstrated that aneurysm- to- parent vessel SR has a significant effect on IA hemodynamics and may be a potential parameter to resolve the confusing trends observed when relating IA rupture risk with absolute IA size.

Supplementary Material

Refer to Web version on PubMed Central for supplementary material.

Acknowledgments

We gratefully acknowledge Kenneth R. Hoffmann, Ph.D., and Petru M. Dinu, B.S., for providing the software for the angiographic geometry reconstruction and Paul H. Dressel, B.F.A., for assisting with the preparation of the illustrations.

Disclosures

This work was supported by the National Science Foundation under Grant BES-0302389; the National Institutes of Health under Grants NS047242, EB002873, and NS043924; and the Brain Aneurysm Foundation. Elad I. Levy, M.D., receives grant support, other research support (devices), and honoraria from Boston Scientific; has an ownership interest in Intratech Medical Ltd. and Micrus Endovascular; serves as a consultant to Cordis Neurovascular, Micrus Endoascular, ev3, and TheraSyn Sensors, Inc.; and receives fees for carotid stent training from Abbott Vascular and ev3. Hui Meng, Ph.D., receives research grants from the National Institutes of Health and National Science Foundation. J Mocco, M.D., M.S., has received a research grant from the Brain Aneurysm Foundation. The other authors have no personal financial or institutional interest in any of the drugs, materials, or devices described in this article.

ABBREVIATIONS

AComA	anterior communicating artery
CFD	computational fluid dynamics
IA	intracranial aneurysm
ICA	internal carotid artery
SR	size ratio
WSS	wall shear stress

References

1. Aaslid R, Markwalder TM, Nornes H. Noninvasive transcranial Doppler ultrasound recording of flow velocity in basal cerebral arteries. J Neurosurg 1982;57:769–774. [PubMed: 7143059]
2. Ausman JI, Roitberg B. A response from the ISUIA. International Study on Unruptured Intracranial Aneurysms. Surg Neurol 1999;52:428–430. [PubMed: 10555853]
3. Beck J, Rohde S, Berkefeld J, Seifert V, Raabe A. Size and location of ruptured and unruptured intracranial aneurysms measured by 3-dimensional rotational angiography. Surg Neurol 2006;65:18–27. [PubMed: 16378842]
4. Brooks DE, Goodwin JW, Seaman GV. Interactions among erythrocytes under shear. J Appl Physiol 1970;28:172–177. [PubMed: 5413303]
5. Burleson AC, Strother CM, Turitto VT. Computer modeling of intracranial saccular and lateral aneurysms for the study of their hemodynamics. Neurosurgery 1995;37:774–784. [PubMed: 8559308]
6. Carter BS, Sheth S, Chang E, Sethl M, Ogilvy CS. Epidemiology of the size distribution of intracranial bifurcation aneurysms: Smaller size of distal aneurysms and increasing size of unruptured aneurysms with age. Neurosurgery 2006;58:217–223. [PubMed: 16462474]
7. Cebral JR, Castro MA, Appanaboyina S, Putman CM, Millan D, Frangi AF. Efficient pipeline for image-based patient-specific analysis of cerebral aneurysm hemodynamics: Technique and sensitivity. IEEE Trans Med Imaging 2005;24:457–467. [PubMed: 15822804]
8. Cebral JR, Castro MA, Burgess JE, Pergolizzi RS, Sheridan MJ, Putman CM. Characterization of cerebral aneurysms for assessing risk of rupture by using patient- specific computational hemodynamics models. AJNR Am J Neuroradiol 2005;26:2550–2559. [PubMed: 16286400]
9. Chang HS. Simulation of the natural history of cerebral aneurysms based on data from the International Study of Unruptured Intracranial Aneurysms. J Neurosurg 2006;104:188–194. [PubMed: 16509491]
10. Clarke G, Mendelow AD, Mitchell P. Predicting the risk of rupture of intracranial aneurysms based on anatomical location. Acta Neurochir (Wien) 2005;147:259–263. [PubMed: 15662565]
11. Dhar S, Tremmel M, Mocco J, Kim M, Yamamoto J, Siddiqui AH, Hopkins LN, Meng H. Morphology parameters for intracranial aneurysm rupture risk assessment. Neurosurgery 2008;63:185–197. [PubMed: 18797347]
12. Ecker RD, Hopkins LN. Natural history of unruptured intracranial aneurysms. Neurosurg Focus 2004;17:E4. [PubMed: 15633981]
13. Forget TR Jr, Benitez R, Veznedaroglu E, Sharan A, Mitchell W, Silva M, Rosenwasser RH. A review of size and location of ruptured intracranial aneurysms. Neurosurgery 2001;49:1322–1326. [PubMed: 11846931]
14. Foutrakis GN, Yonas H, Sclabassi RJ. Saccular aneurysm formation in curved and bifurcating arteries. AJNR Am J Neuroradiol 1999;20:1309–1317. [PubMed: 10472991]
15. Gonzalez CF, Cho YI, Ortega HV, Moret J. Intracranial aneurysms: Flow analysis of their origin and progression. AJNR Am J Neuroradiol 1992;13:181–188. [PubMed: 1595440]
16. Hassan T, Timofeev EV, Saito T, Shimizu H, Ezura M, Matsumoto Y, Takayama K, Tominaga T, Takahashi A. A proposed parent vessel geometry-based categorization of saccular intracranial

aneurysms: Computational flow dynamics analysis of the risk factors for lesion rupture. J Neurosurg 2005;103:662–680. [PubMed: 16266049]

17. Hoi Y, Meng H, Woodward SH, Bendok BR, Hanel RA, Guterman LR, Hopkins LN. Effects of arterial geometry on aneurysm growth: Three- dimensional computational fluid dynamics study. J Neurosurg 2004;101:676–681. [PubMed: 15481725]
18. International Study of Unruptured Intracranial Aneurysms Investigators. Unruptured intracranial aneurysms—Risk of rupture and risks of surgical intervention. N Engl J Med 1998;339:1725–1733. [PubMed: 9867550]
19. Jou LD, Wong G, Dispensa B, Lawton MT, Higashida RT, Young WL, Saloner D. Correlation between lumenal geometry changes and hemodynamics in fusiform intracranial aneurysms. AJNR Am J Neuroradiol 2005;26:2357–2363. [PubMed: 16219845]
20. Juvela S, Porras M, Poussa K. Natural history of unruptured intracranial aneurysms: Probability of and risk factors for aneurysm rupture. J Neurosurg 2000;93:379–387. [PubMed: 10969934]
21. Kailasnath P, Dickey P. ISUIA-II: The need to share more data. Surg Neurol 2004;62:95. [PubMed: 15261493]
22. Malek AM, Alper SL, Izumo S. Hemodynamic shear stress and its role in atherosclerosis. JAMA 1999;282:2035–2042. [PubMed: 10591386]
23. Meng H, Swartz DD, Wang Z, Hoi Y, Kolega J, Metaxa EM, Szymanski MP, Yamamoto J, Sauvageau E, Levy EI. A model system for mapping vascular responses to complex hemodynamics at arterial bifurcations in vivo. Neurosurgery 2006;59:1094–1101. [PubMed: 17143243]
24. Meng H, Wang Z, Hoi Y, Gao L, Metaxa E, Swartz DD, Kolega J. Complex hemodynamics at the apex of an arterial bifurcation induces vascular remodeling resembling cerebral aneurysm initiation. Stroke 2007;38:1924–1931. [PubMed: 17495215]
25. Meng H, Wang Z, Kim M, Ecker RD, Hopkins LN. Saccular aneurysms on straight and curved vessels are subject to different hemodynamics: Implications of intravascular stenting. AJNR Am J Neuroradiol 2006;27:1861–1865. [PubMed: 17032857]
26. Mocco J, Komotar RJ, Lavine SD, Meyers PM, Connolly ES, Solomon RA. The natural history of unruptured intracranial aneurysms. Neurosurg Focus 2004;17:E3. [PubMed: 15633980]
27. Nedeltchev K, Arnold M, Nirkko A, Sturzenegger M, Rihs F, Bühler R, Mattle HP. Changes in blood flow velocity in the middle and anterior cerebral arteries evoked by walking. J Clin Ultrasound 2002;30:132–138. [PubMed: 11948568]
28. Orz Y, Kobayashi S, Osawa M, Tanaka Y. Aneurysm size: A prognostic factor for rupture. Br J Neurosurg 1997;11:144–149. [PubMed: 9156002]
29. Perktold K, Peter RO, Resch M, Langs G. Pulsatile non- Newtonian blood flow in three-dimensional carotid bifurcation models: A numerical study of flow phenomena under different bifurcation angles. J Biomed Eng 1991;13:507–515. [PubMed: 1770813]
30. Raghavan ML, Ma B, Harbaugh RE. Quantified aneurysm shape and rupture risk. J Neurosurg 2005;102:355–362. [PubMed: 15739566]
31. Rinkel GJ, Djibuti M, Algra A, van Gijn J. Prevalence and risk of rupture of intracranial aneurysms: A systematic review. Stroke 1998;29:251–256. [PubMed: 9445359]
32. Shojima M, Oshima M, Takagi K, Torii R, Hayakawa M, Katada K, Morita A, Kirino T. Magnitude and role of wall shear stress on cerebral aneurysm: Computational fluid dynamic study of 20 middle cerebral artery aneurysms. Stroke 2004;35:2500–2505. [PubMed: 15514200]
33. Steinman DA, Milner JS, Norley CJ, Lownie SP, Holdsworth DW. Image-based computational simulation of flow dynamics in a giant intracranial aneurysm. AJNR Am J Neuroradiol 2003;24:559–566. [PubMed: 12695182]
34. Tian F, Ouyang S, Yang Q. Effect of thinking on intracranial blood flow velocities. Chin Med J (Engl) 2001;114:1211–1212. [PubMed: 11729523]
35. Ujiie H, Sato K, Onda H, Oikawa A, Kagawa M, Takakura K, Kobayashi N. Clinical analysis of incidentally discovered unruptured aneurysms. Stroke 1993;24:1850–1856. [PubMed: 8248967]
36. Ujiie H, Tachibana H, Hiramatsu O, Hazel AL, Matsumoto T, Ogasawara Y, Nakajima H, Hori T, Takakura K, Kajiya F. Effects of size and shape (aspect ratio) on the hemodynamics of saccular aneurysms: A possible index for surgical treatment of intracranial aneurysms. Neurosurgery 1999;45:119–130. [PubMed: 10414574]

37. Ujiie H, Tamano Y, Sasaki K, Hori T. Is the aspect ratio a reliable index for predicting the rupture of a saccular aneurysm? Neurosurgery 2001;48:495–503. [PubMed: 11270538]

38. Weir, B. Aneurysms Affecting the Nervous System. Baltimore: Williams & Wilkins; 1987. p. 308-363.

39. Weir B, Amidei C, Kongable G, Findlay JM, Kassell NF, Kelly J, Dai L, Karrison TG. The aspect ratio (dome/neck) of ruptured and unruptured aneurysms. J Neurosurg 2003;99:447–451. [PubMed: 12959428]

40. Weir B, Disney L, Karrison T. Sizes of ruptured and unruptured aneurysms in relation to their sites and the ages of patients. J Neurosurg 2002;96:64–70. [PubMed: 11794606]

41. Wiebers DO, Whisnant JP, Huston J 3rd, Meissner I, Brown RD Jr, Piepgras DG, Forbes GS, Thielen K, Nichols D, O'Fallon WM, Peacock J, Jaeger L, Kassell NF, Kongable-Beckman GL, Torner JC. Unruptured intracranial aneurysms: Natural history, clinical outcome, and risks of surgical and endovascular treatment. Lancet 2003;362:103–110. [PubMed: 12867109]

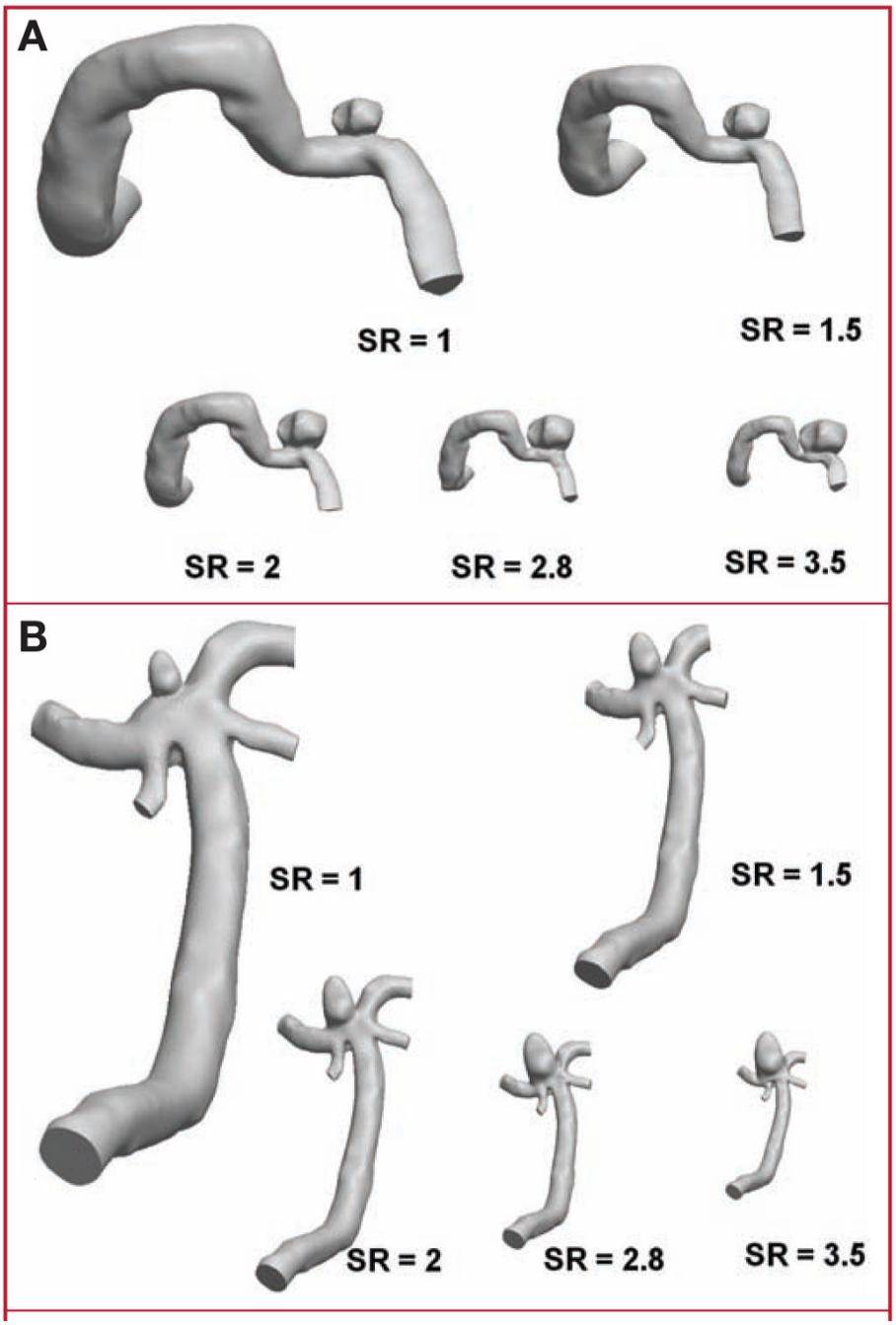

FIGURE 1.
Drawings showing geometry models of experiment 1 (constant intracranial aneurysm [IA] size and varying size ratio [SR]). **A,** sidewall IA case; **B,** terminal IA case.

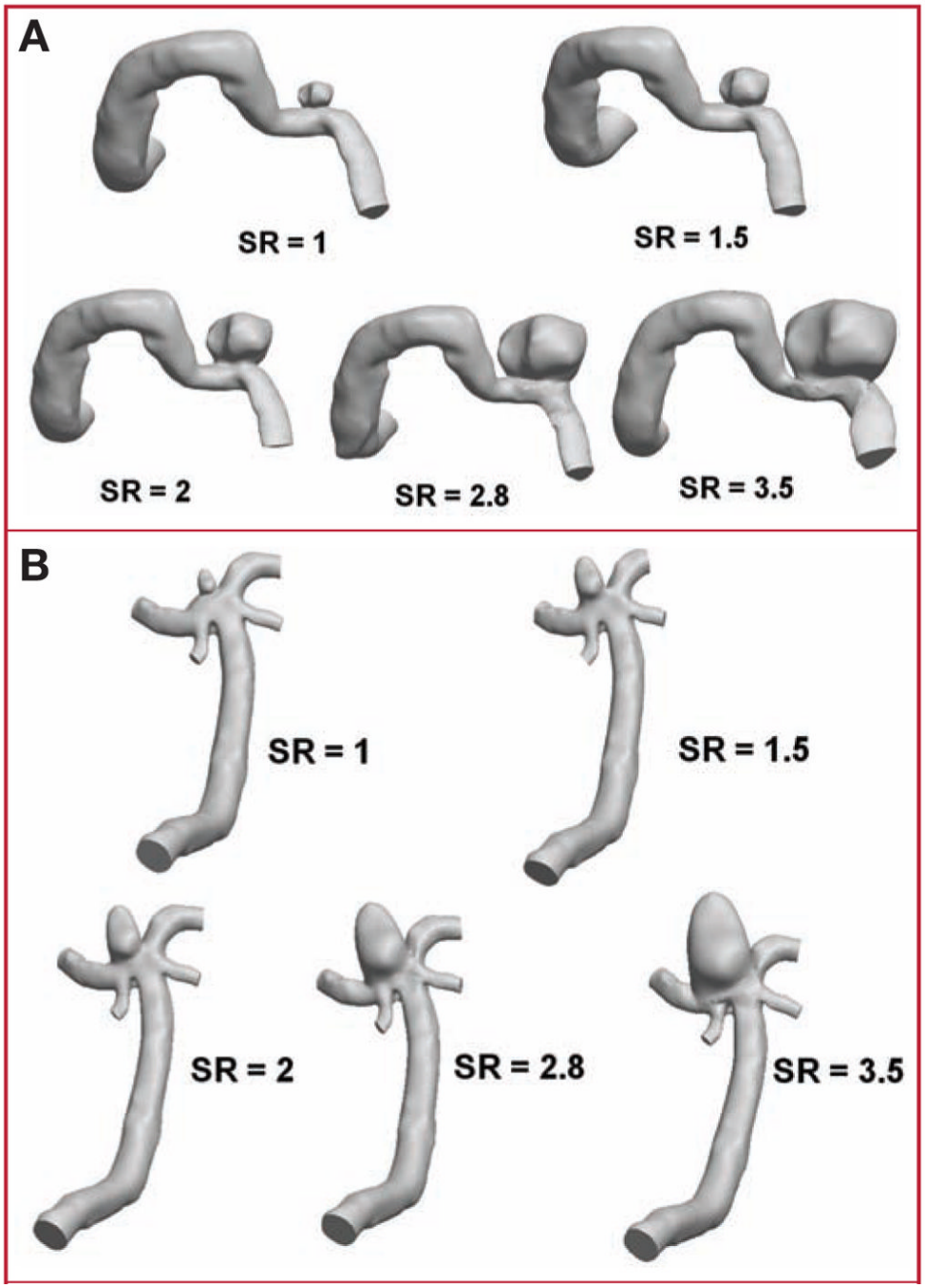

FIGURE 2.
Drawings showing geometry models of experiment 2 (constant vessel size and varying SR). **A**, sidewall IA case; **B**, terminal IA case.

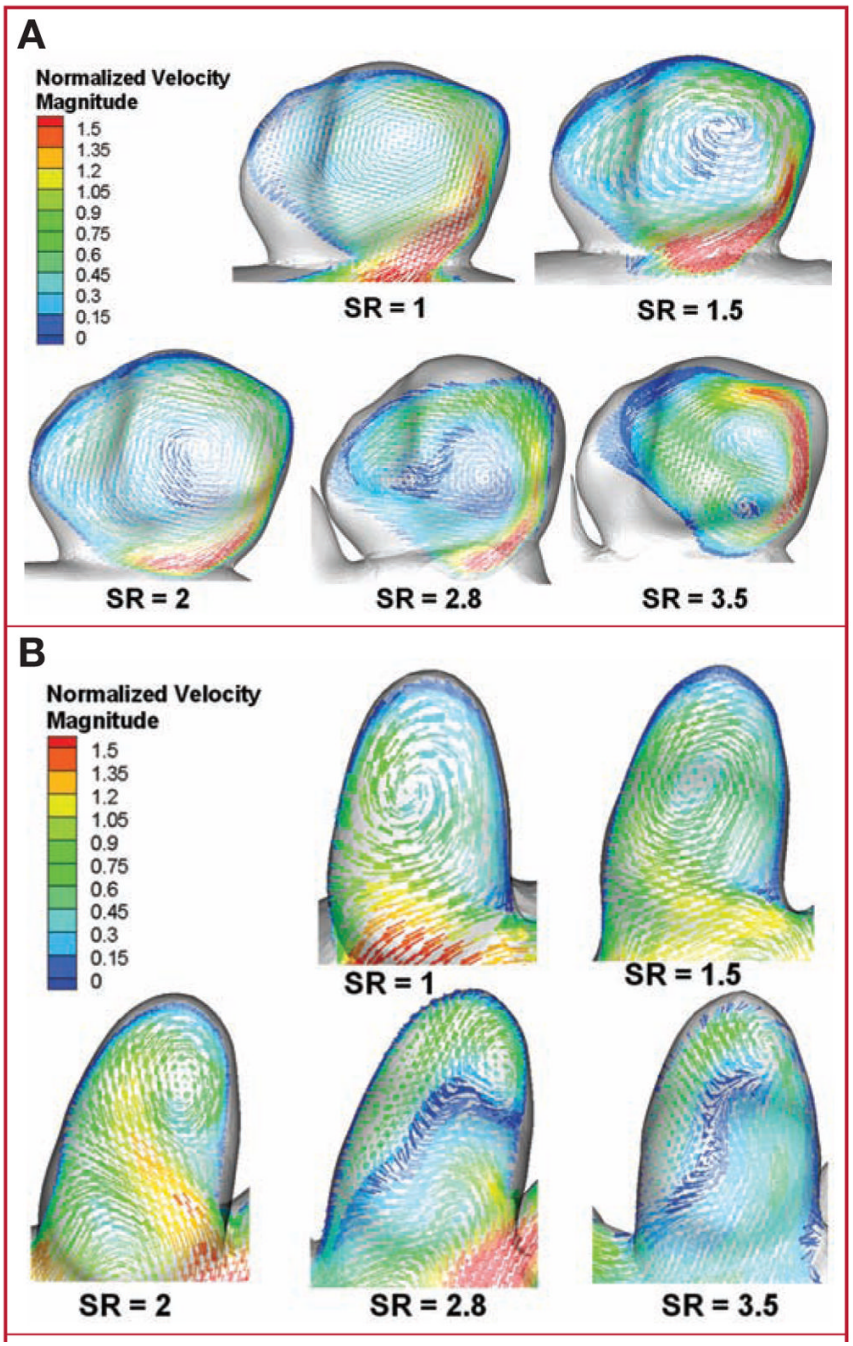

FIGURE 3.

Drawings showing intra- aneurysmal flow patterns (time averaged) from experiment 1 illustrated by vector plots on planes cutting through the aneurysm volume for sidewall IA (**A**) and terminal (**B**) IA cases. Velocities are normalized with the corresponding inlet velocity, thereby allowing comparison of **A** and **B**. Vector lengths have been held constant to enhance visibility of vortex structures; color scales indicate velocity magnitude. Flow patterns change from a simple, single vortex to multiple vortices when SR is more than 2. Time-dependent animations of the intra-aneurysmal flow over a cardiac cycle have been included as supplemental files (see Videos, Supplementary Digital Content 1,

http://links.lww.com/A779, and Supplementary Digital Content 2, http://links.lww.com/A780). Dynamics of the vortices observed can be seen in the animations.

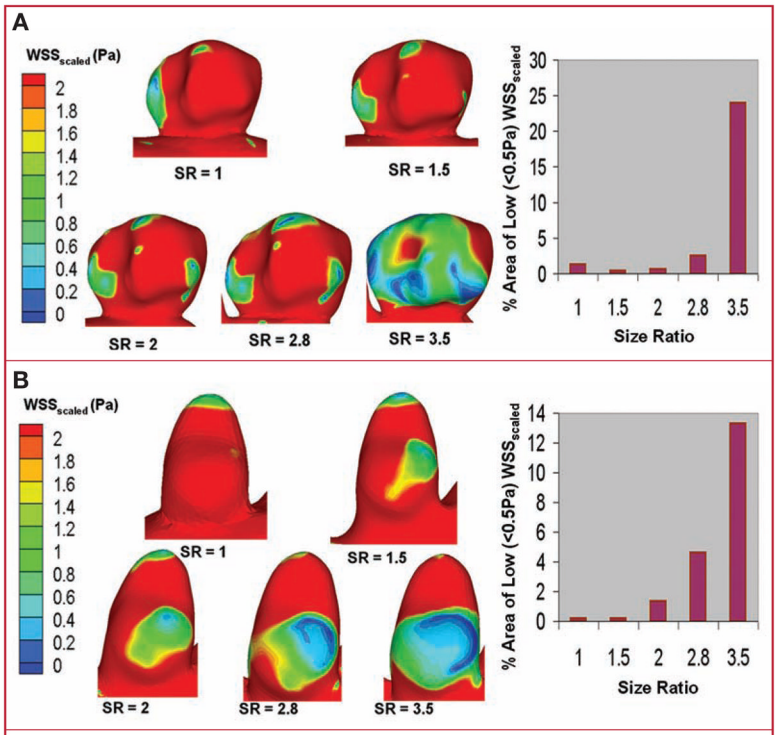

FIGURE 4.

Surface plots of scaled wall shear stress (WSS_{scaled}) on the aneurysmal walls in experiment 1 showing an increase in the area exposed to low WSS_{scaled} (<0.5 Pa) with increasing SR for sidewall (**A**) and terminal (**B**) IA cases.

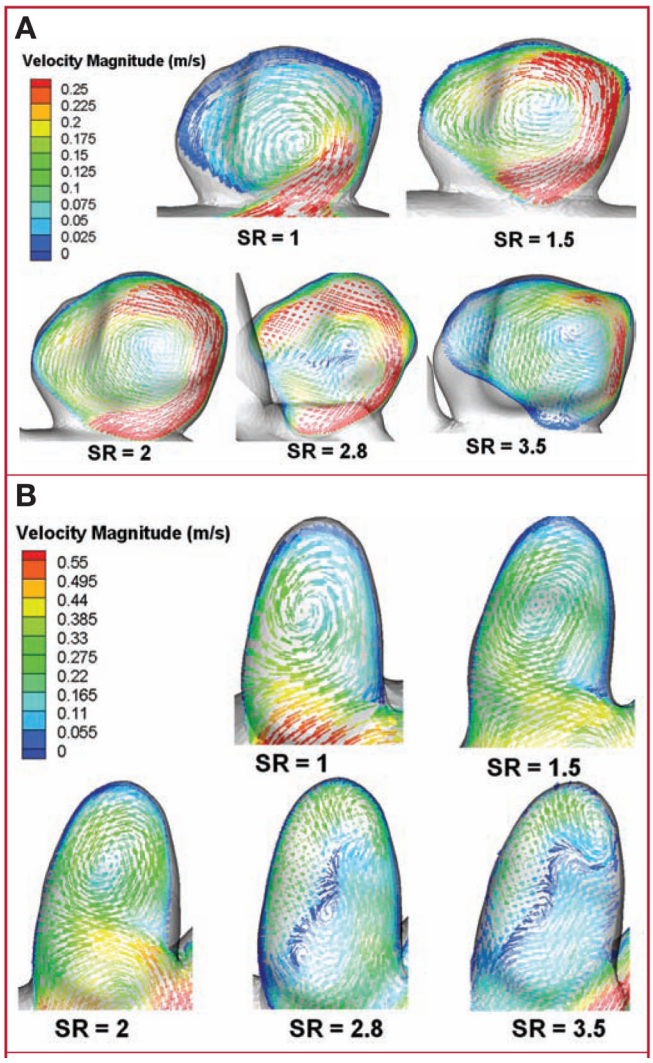

FIGURE 5.

Drawings showing intra-aneurysmal flow patterns (time averaged) from experiment 2 illustrated by vector plots on planes cutting through the aneurysm volume for sidewall IA (**A**) and terminal (**B**) IA cases. Vector lengths have been held constant to enhance visibility of vortex structures; color scales indicate velocity magnitude. Flow patterns change from a simple, single vortex to multiple vortices when SR is more than 2. Time- dependent animations of the intra- aneurysmal flow over a cardiac cycle have been included as supplemental files (see Videos, Supplementary Digital Content 3, http://links.lww.com/A781, and Supplementary Digital Content 4, http://links.lww.com/A782). Dynamics of observed vortices can be seen in the animations.

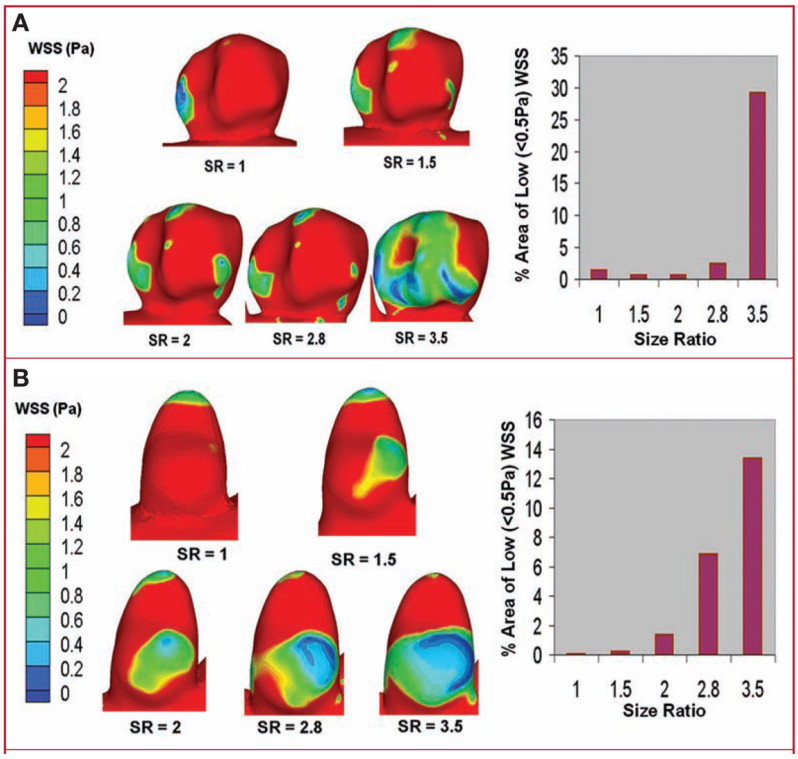

FIGURE 6.

Surface plots of WSS on aneurysmal walls in experiment 2 showing an increase in the area exposed to low WSS (<0.5 Pa) with increasing SR for sidewall (**A**) and terminal (**B**) IA cases.